**The EMBO Journal** Vol.18 No.8 pp.2031–2039, 1999

# Crystal structure of baculovirus P35: role of a novel reactive site loop in apoptotic caspase inhibition

**Andrew J.Fisher[1], Wilfred dela Cruz, Stephen J.Zoog[2], Christine L.Schneider[2] and Paul D.Friesen[2]**

Department of Chemistry and Section of Molecular and Cellular Biology, University of California, Davis, CA 95616 and [2]Institute for Molecular Virology and Department of Biochemistry, University of Wisconsin, Madison, WI 53706, USA

[1]Corresponding author
e-mail: fisher@chem.ucdavis.edu

**The aspartate-specific caspases are critical protease effectors of programmed cell death and consequently represent important targets for apoptotic intervention. Baculovirus P35 is a potent substrate inhibitor of metazoan caspases, a property that accounts for its unique effectiveness in preventing apoptosis in phylogenetically diverse organisms. Here we report the 2.2 Å resolution crystal structure of P35, the first structure of a protein inhibitor of the death caspases. The P35 monomer possesses a solvent-exposed loop that projects from the protein's main β-sheet core and positions the requisite aspartate cleavage site at the loop's apex. Distortion or destabilization of this reactive site loop by site-directed mutagenesis converted P35 to an efficient substrate which, unlike wild-type P35, failed to interact stably with the target caspase or block protease activity. Thus, cleavage alone is insufficient for caspase inhibition. These data are consistent with a new model wherein the P35 reactive site loop participates in a unique multi-step mechanism in which the spatial orientation of the loop with respect to the P35 core determines post-cleavage association and stoichiometric inhibition of target caspases.**

*Keywords*: apoptosis/baculovirus/caspase inhibitor/crystallography/P35

## Introduction

Apoptosis, or programmed cell death, is a multi-step, signal-induced mechanism for cellular destruction. It is a highly regulated suicide process that is crucial for normal development, tissue homeostasis and defense from foreign pathogens, including viruses (Steller, 1995; Hardwick, 1997; Jacobson *et al*., 1997). Aberrant or misregulated apoptosis is associated with tumorigenesis, degenerative diseases and virus pathogenesis (Thompson, 1995). The components of the death apparatus are well conserved and include the caspases, a family of cysteinyl proteases that are critical apoptotic effectors (Hengartner and Horvitz, 1994; Martin and Green, 1995; Fraser and Evan, 1996; Nicholson and Thornberry, 1997; Cryns and Yuan, 1998). After proteolytic activation from their proenzyme form, these aspartate-specific proteases induce nuclear and cytoplasmic condensation, internucleosomal DNA fragmentation, cytoskeletal rearrangements and plasma membrane blebbing, all morphological hallmarks of apoptosis. The diversity of anti-apoptotic proteins that affect either caspase activation or activity indicates that these death proteases provide a decisive control point in the commitment to apoptotic death (White, 1996; Villa *et al*., 1997; Cryns and Yuan, 1998).

In a strategy to block host cell defenses and promote multiplication, viruses have evolved diverse anti-apoptotic genes that regulate the cell death machinery (Shen and Shenk, 1995; Hardwick, 1997; O'Brien, 1998). Baculovirus *p35* is of particular interest since it not only blocks virus-induced apoptosis (Clem *et al*., 1991), but also functions as a general and effective suppressor of programmed cell death in diverse organisms when expressed ectopically (Rabizadeh *et al*., 1993; Cartier *et al*., 1994; Hay *et al*., 1994; Sugimoto *et al*., 1994; Beidler *et al*., 1995; Martinou *et al*., 1995; Robertson *et al*., 1997). This feature has been exploited in a promising first example of anti-apoptosis therapy in which eye-specific expression of *p35* prevents blindness in retinal degeneration mutants of *Drosophila* (Davidson and Steller, 1998).

Accounting for its broad effectiveness as an apoptotic suppressor, protein P35 is a potent inhibitor of group I, II and III caspases (Bump *et al*., 1995; Xue and Horvitz, 1995; Bertin *et al*., 1996; Zhou *et al*., 1998). Lacking sequence similarity to any known protease regulators including the serpins, this 299 residue protein is a substrate inhibitor in which cleavage at Asp87 of the caspase recognition sequence 84-DQMD↓G-88 is correlated with caspase inhibition. Asp87 is a critical residue since replacement causes loss of P35 anti-apoptotic activity and abrogates *in vitro* caspase inhibition (Xue and Horvitz, 1995; Bertin *et al*., 1996). Upon stoichiometric inhibition of human caspase-1, the 10 and 25 kDa cleavage products of P35 remained stably associated with the inhibited caspase (Bump *et al*., 1995). This finding suggested that P35 acts as an irreversible, or slowly reversible suicide inhibitor. In an alternative model, P35 may act as a competitive inhibitor if present at sufficiently high levels (Xue and Horvitz, 1995). Thus, the mechanism by which P35 accomplishes broad specificity caspase inhibition *in vivo* remains unresolved.

To define the molecular mechanism by which baculovirus P35 functions as a potent substrate inhibitor of the death caspases, we have determined its three-dimensional structure. We report here the 2.2 Å resolution crystal structure of active P35 prior to caspase cleavage. The structure provides new insight into a multi-step mechanism of caspase inhibition and opens the door to novel P35 designs for use in anti-caspase therapeutic approaches.

## Results

### *Overall structure*

P35 crystallized with three monomers in the crystallographic asymmetric unit, designated A, B and C. The

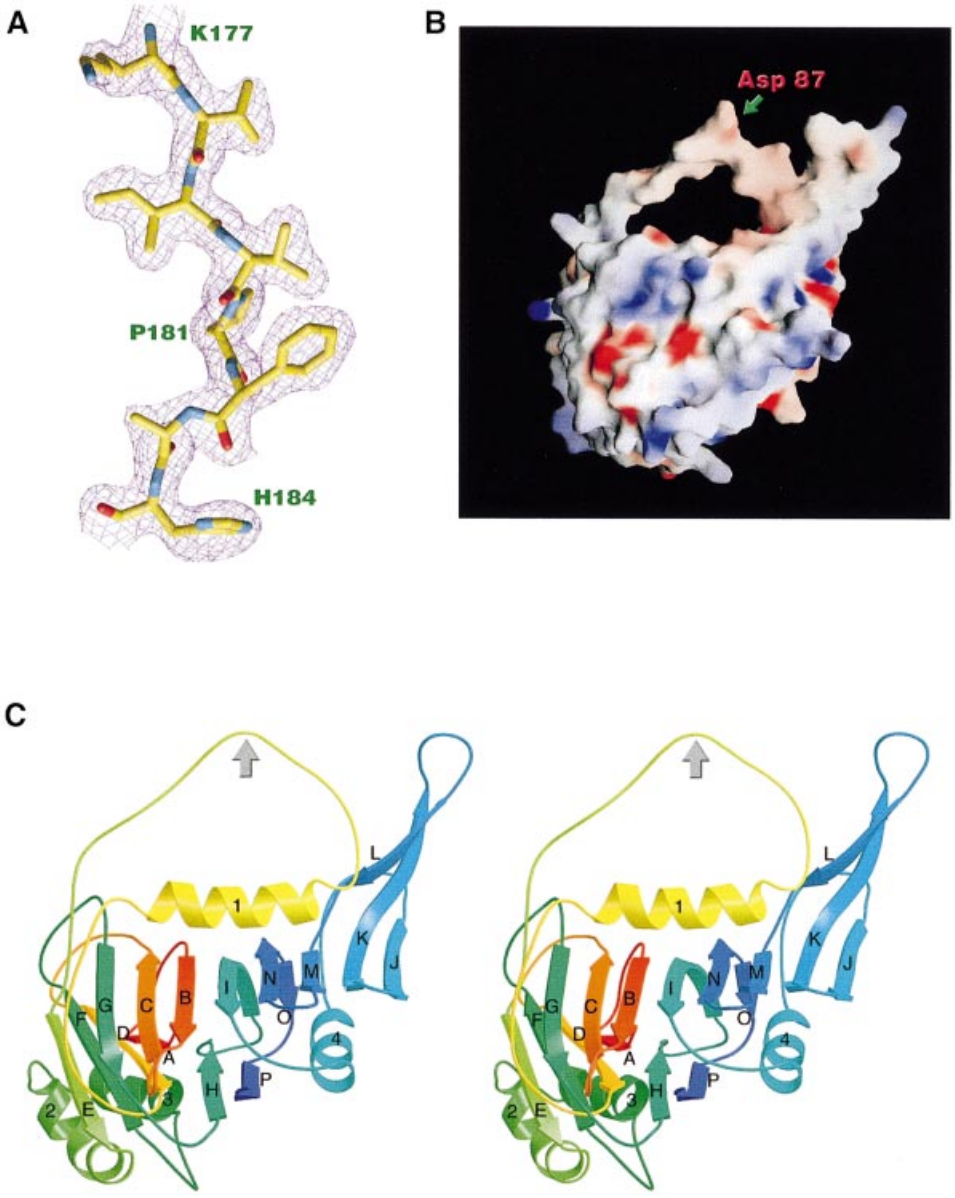


**Fig. 1.** P35 structure. (**A**) Representative section of the final electron density map (contoured at 1σ) calculated with coefficients of $2|F_o| - |F_c|$ and phases computed from the final refined model. The protein region corresponds to the end of βH and the following loop. The figure was generated by the program MOLVIEW (Smith, 1995). (**B**) Electrostatic molecular surface rendering of the P35 monomer demonstrating the completely solvent-exposed portion of the reactive site loop (generated by the program GRASP, Nicholls *et al*., 1991). Surfaces are colored by electrostatic charge, with positive and negative regions in blue and red respectively. The location of Asp87 ($P_1$ residue) is labeled. (**C**) Stereo ribbon drawing of P35 monomer B. The color scheme varies through the rainbow spectrum, starting at red for the N-terminus and ending with violet at the C-terminus. The P35 reactive site loop, which is cleaved by the caspases, is the solvent-exposed loop at the top of the protein as viewed. The scissile bond is marked with an arrow. The cellulose-binding domain fold corresponds to the β-barrel subdomain at the left portion of the structure. Figures 1C, 2, 3A and 4 were created with the program MOLSCRIPT (Kraulis, 1991).

structure was determined by multiple isomorphous replacement (MIR) at 2.9 Å resolution and refined against 2.2 Å resolution synchrotron data. The P35 monomer structure consists of a novel single domain globular protein with overall dimensions of ~45×55×40 Å. The central core of the structure consists of an eight-stranded mostly antiparallel β-sheet (Figure 1). Strands βB and βI run parallel in this notably flat β-sheet. Strands βA, βD, βE and βF lie below β-strands βB, βC and βG of the central β-sheet to form a seven-stranded antiparallel β-barrel with structure and topology similar to the cellulose-binding domain (see below). Helices α2 and α3 form an antiparallel helix–turn–helix motif and lie below the cellulose-binding domain. Helix α2 bends at Lys114 to allow for the tight α2–α3 turn and helix packing against the core region.

The striking feature of the P35 structure is a large loop domain (residues 60–98), designated the reactive site loop, that protrudes above the central β-sheet core. The loop begins with a single α-helix (α1) that traverses the top of the central sheet and is succeeded by the $P_4$–$P_{1'}$ residues (84-DQMD↓G-88) that represent the caspase recognition site. The caspase cleavage site, Asp87–Gly88 ($P_1$ and $P_{1'}$ residues), comprises the apex of the loop, which is solvent exposed and fully accessible to the target caspase. The position of the reactive site loop is determined in part by amphipathic helix α1 that packs

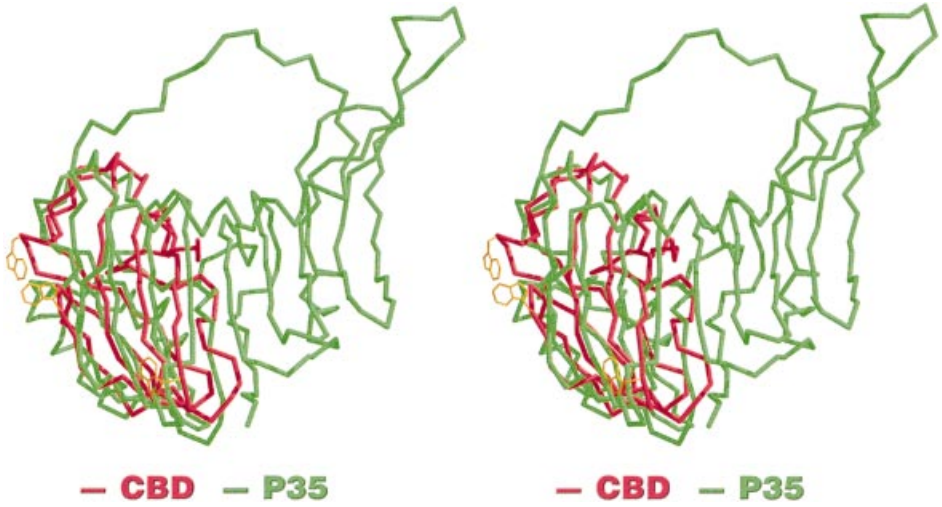


**Fig. 2.** Stereo superposition of P35 (drawn in green) on the cellulose-binding domain from β-1,4-xylanase (drawn in red) (PDB accession code 1EXG). While no protein structure had an overall fold comparable with that of the P35 core domain, the N-terminal portion of P35 displayed structural similarities to the type II CBD (Xu *et al*., 1995). The CBD superimposes onto P35 with an r.m.s. deviation of 2.8 Å for 90 equivalent α-carbons. The three CBD tryptophan residues implicated in binding cellulose are drawn with orange bonds. The corresponding residues in P35 are different.

against the β-sheet at an unusual angle that is perpendicular to the strands of the core β-sheet. The hydrophobic residues of the helix interact with the hydrophobic residues from the central β-sheet, and the hydrophilic residues of α1 are exposed to solvent. Strand βK extends past the central β-sheet and turns upward to form a β-hairpin with βL that lies adjacent to the reactive site loop. The structure predicts that Tyr260 and Trp262 of βL make hydrophobic interactions with Tyr82 of the reactive site loop to stabilize the loop. These interactions are observed in all three monomers in the asymmetric unit. The last four strands of the central β-sheet (βJ, βK, βM and βN) organize into a β-meander motif. Strands βH and βP along with helix α4 pack underneath the right hand portion of the central eight-stranded β-sheet as viewed in Figure 1. Since the last residue observed is Lys299, the C-terminal $His_6$-Tag is disordered in all three monomers.

### *Correlation between P35 structure and function*

The biological relevance of this P35 structure is strongly supported by previous genetic analyses, including in-frame two-codon (Ala–Ser) insertional mutagenesis (Bertin *et al*., 1996). Examination of the crystal structure revealed a striking correlation between mutational disruption of defined secondary structures and the loss of P35 function. For example, all insertions located within β-sheets (in10, in28, in105, in152, in197, in278 and in290) and within α-helices (in74 and in130) caused loss of function. In contrast, mutations (in145, in174, in205, in223, in240, in254 and in273) located within intervening loops that could accommodate insertions without disruption of adjacent secondary structure had no phenotypic effect. Thus, the observed pattern in which disruption of defined secondary structure caused loss of function, but insertions within intervening loops exerted little if any effect, suggests that the structure of P35 as determined here represents a biologically relevant structure of this protein.

### *Cellulose-binding domain similarity*

The P35 structure was used as a search model to probe a three-dimensional structural database to find similar folds (Holm and Sander, 1993). While no protein structure had an overall fold comparable with that of the P35 core domain, the N-terminal portion of P35 displayed structural similarities to the type II cellulose-binding domains (CBD) (Xu *et al*., 1995). The biological significance of this intriguing structural similarity is unknown. P35 exhibits no sequence similarity to any class of cellulose-binding proteins. The CBD similarity in P35 corresponds to the seven-stranded antiparallel β-barrel made up of β-strands A–G. This barrel superimposes on the CBD of β-1,4-xylanase/glucanase from the bacterium *Cellulomonas fimi* with an r.m.s. deviation of 2.8 Å for 90 equivalent α-carbons, as calculated by the program LSQKAB (Kabsch, 1976) (Figure 2). The topology of CBD is identical to the cellulose-binding motif of P35 with the exception of strand βA. In P35, this strand is at the N-terminus, whereas in CBD the structurally equivalent strand comes from the C-terminus of the protein. Nonetheless, the directionality of all strands is identical. P35 also contains two large insertions not found in CBD. The reactive site loop, consisting of helix α1 and the solvent-exposed caspase target site, is inserted between strands βD and βE. Also, the two antiparallel helices α2 and α3 positioned below the CBD are inserted between strands βE and βF. In spite of the sequence and structural differences, P35 does have an affinity for cellulose, with a dissociation constant of ~3 μM (data not shown).

### *Flexibility of the reactive site loop*

Part of the unusual reactive site loop of P35 extends away from the main β-core and is completely solvent exposed. This reactive loop functions as the primary recognition site for the target caspases. Strict non-crystallographic symmetry (NCS), which was constrained during the early

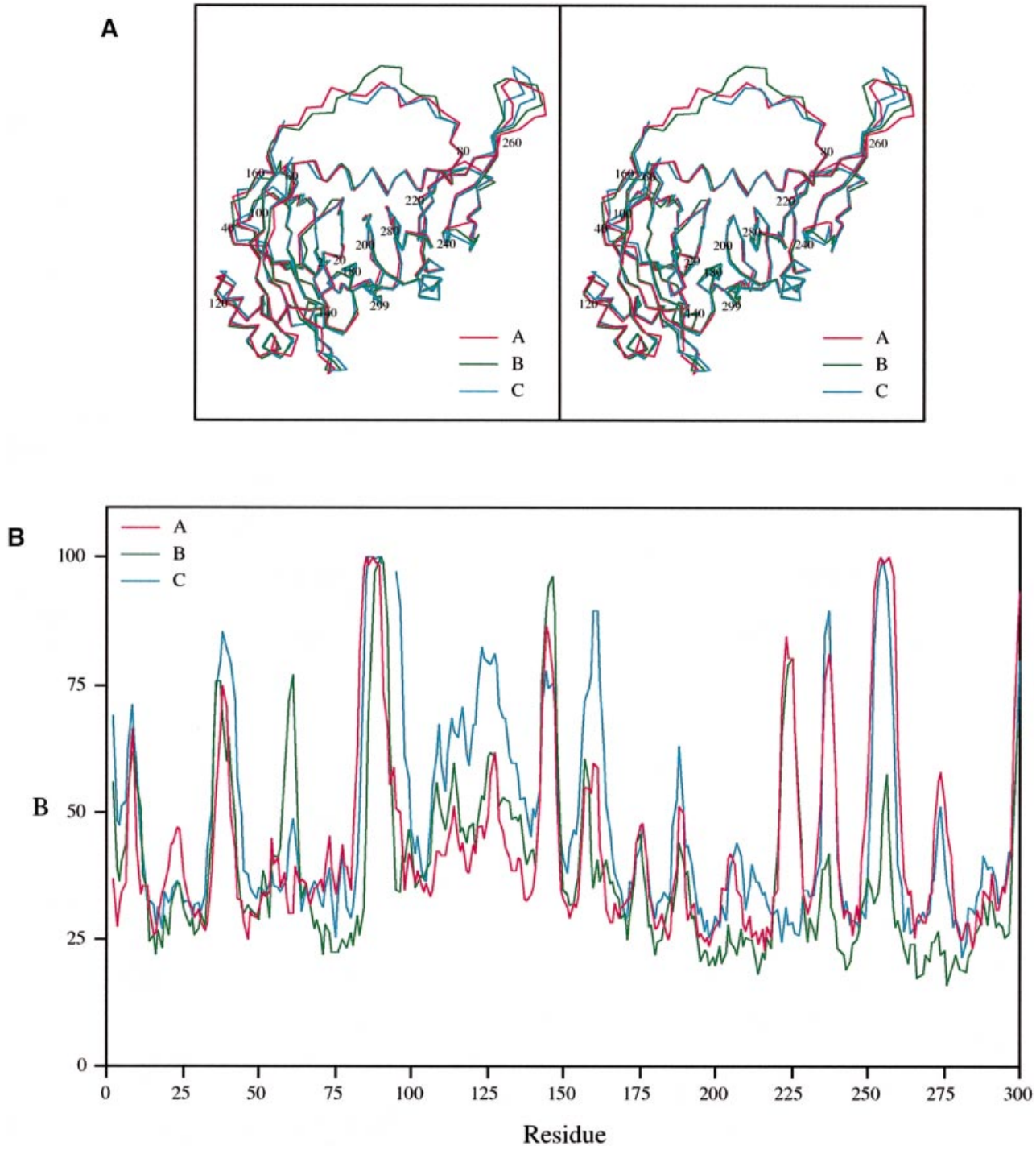


**Fig. 3.** (**A**) Stereo drawing illustrating the superposition of the three P35 monomers observed in the crystal asymmetric unit. The α-carbon tracings of the A, B and C monomers are illustrated in red, green and blue, respectively. The largest structural differences are observed in the solvent-exposed region of the reactive site loop and the adjacent βK–βL hairpin loop. (**B**) Plot of the averaged main chain temperature factors for the three P35 monomers in the asymmetric unit, A, B and C colored red, green and blue, respectively. Electron density clearly defined all main chain atoms except for residues 90–95 of the C monomer.

stages of structural refinement, was relaxed, resulting in a better agreement between the model and both the working and cross-validated data. This improved the electron density map to model the solvent-exposed segment of the reactive site loop (residues 84–95) and the adjacent hairpin loop between strands βK and βL (residues 252–259). All three monomers in the asymmetric unit are very similar in structure, with the largest deviations occurring at these two loop regions. The loop displacements, which culminate up to 5.7 Å at the apex of the reactive site loop, result from the three distinct crystal packing environments in the asymmetric unit (Figure 3A). The observed variances, along with weak electron density and high crystallographic temperature values that define

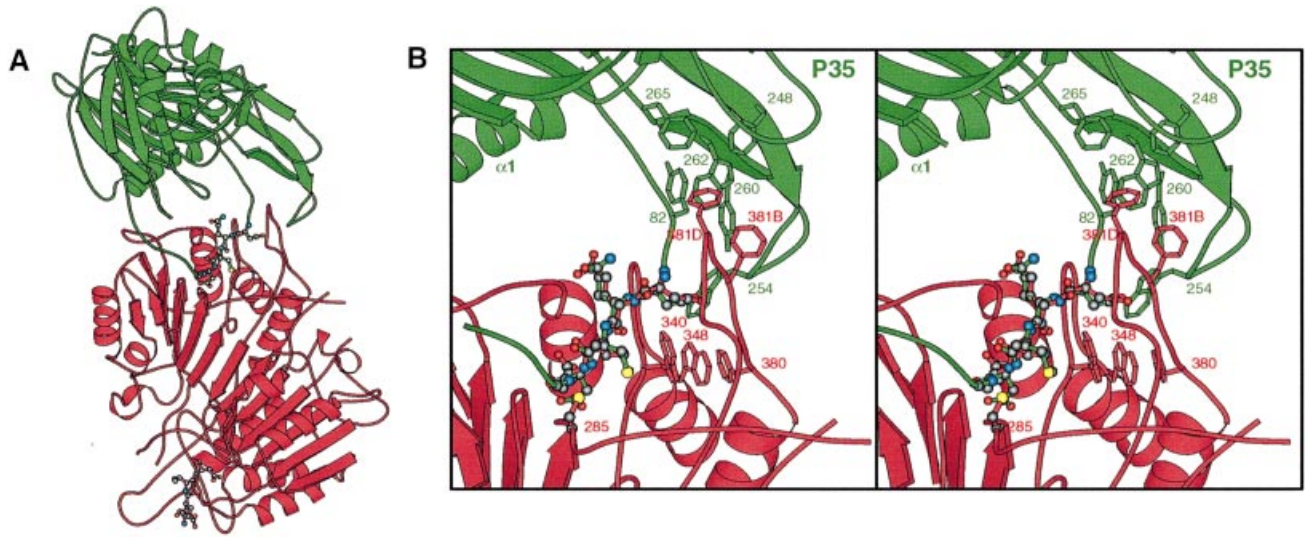


**Fig. 4.** P35 docked into the active site of caspase-3. (**A**) Ribbon view of P35 (green) modeled into the active site of caspase-3 (drawn in red). The superposition of P35 residues 84-DQMD-87 onto the tetrapeptide DEVD aldehyde inhibitor bound in the active site of caspase-3 (PDB accession file 1PAU) helped guide the model of the docking. (**B**) Close-up view of the P35 modeled into the active site of caspase-3 (same orientation as in A). The backbone atoms of P35 84-DQMD-87 (displayed as ball-and-stick with green bonds) superimpose with an r.m.s. deviation of 0.72 Å onto the aldehyde tetrapeptide inhibitor DEVD (displayed as ball-and-stick with red bonds) bound in the caspase-3 active site. The active site Cys285 in caspase-3 is shown. The aromatic residues in the βK–βL loop of P35 and the extended loop in the vicinity of residue 381 in caspase-3 are displayed as sticks in their respective colors.

these loops, indicate flexibility and/or conformational latitude amid residues in these loops (Figure 3B). Despite plasticity, the reactive site loop extends from the main β-core and is completely solvent exposed in all three P35 monomers (Figure 3A). The inherent flexibility of the loop, which includes the caspase recognition residues, may contribute to P35's broad specificity as a caspase inhibitor.

### *P35 interaction with caspase*

A current model for P35 anti-apoptotic activity proposes that P35 inhibits caspase activity by a mechanism wherein cleavage at Asp87 leads to formation of a stable P35–caspase complex (Bump *et al*., 1995; Bertin *et al*., 1996; Zhou *et al*., 1998). To examine possible P35–caspase interactions, we superimposed the main chain atoms of the P35 $P_4$–$P_1$ cleavage residues (84-DQMD-87) with those of the tetrapeptide inhibitor DEVD-CHO bound in the active site of human caspase-3, a known target of P35 for which the structure is known (Rotonda *et al*., 1996; Mittl *et al*., 1997). The superposition made it possible to generate a model of pre-cleaved P35 complexed with caspase-3 (Figure 4A). The $P_4$–$P_1$ residues of P35 fit well within the caspase-3 active site with no obvious steric hindrances, due in part to the sharp turn at the scissile bond between Asp87 and Gly88 (Figure 4B).

A feature of this P35–caspase-3 modeled pre-cleavage complex is the limited number of interactions and contacts between P35 and caspase-3 due to the outstretched solvent-exposed reactive site loop, which is observed with all three P35 monomers in the asymmetric unit. The model does propose potential hydrophobic interactions, adjacent to the active site, between the P35 βK–βL hairpin loop and a loop at residue 381 in caspase-3. However, this caspase loop is significantly different between the major subfamilies of caspases based on sequence alignments and structural analysis of human caspase-1 and caspase-3 (Rotonda *et al*., 1996; Mittl *et al*., 1997). Caspase-3 contains a 10 residue insert at a position equivalent to residue 381 in caspase-1. This caspase loop contributes to the $S_4$ binding pocket that defines the $P_4$ residue specificity. In the modeled complex with P35, this loop contains many aromatic residues that lie in close proximity to aromatic residues in the βK–βL loop of P35 (Figure 4B). Trp262 of P35 is 4.3 and 3.9 Å away from Phe381B and Phe381D, respectively in caspase-3 (the caspase-3 numbering scheme is that used in PDB file 1PAU which was used to facilitate easier comparisons with caspase-1). A small post-cleavage conformational change in either the caspase-3 381 insertion loop or the P35 βK–βL hairpin loop could promote hydrophobic interactions between these loops. Nonetheless, it is unlikely that these potential interactions contribute to the high affinity of P35 for caspase ($K_i$ = 100 pM) (Zhou *et al*., 1998) since P35 effectively inhibits caspases lacking this loop. The potency of P35 as an inhibitor of group I, II and III caspases (Zhou *et al*., 1998) argues that P35 inhibition involves a structural or mechanistic feature shared among the caspases and a stabilization of interactions between P35 and the target caspases.

### *Requirement for cleavage site Asp87 for caspase association*

To define the molecular determinants of stable interaction between P35 and caspase, we tested the contribution of the reactive site loop and its critical $P_1$ cleavage residue Asp87, both of which make initial contact with the caspase. When mixed with human caspase-3 overproduced in insect cells, the wild-type P35-$His_6$ crystallized here was cleaved to generate the signature 10 and 25 kDa fragments (Figure 5A and B). In contrast, caspase-3 failed to cleave D87A-mutated P35-$His_6$ (lane 5) in which Asp87 was replaced with alanine, a loss-of-function mutation (Xue and Horvitz, 1995; Bertin *et al*., 1996). Both caspase-3 subunits (p17

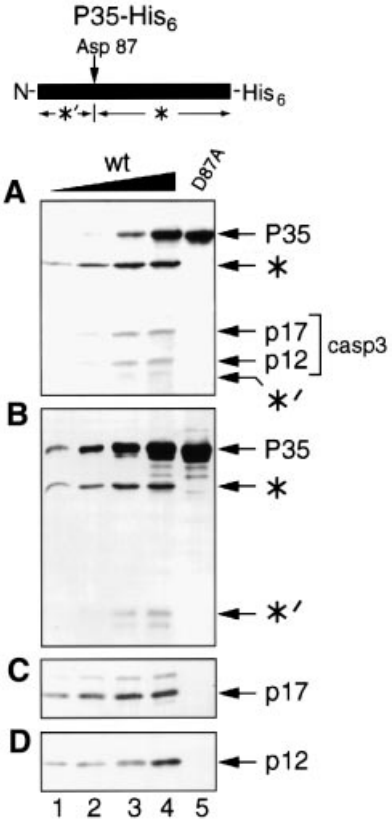


**Fig. 5.** Post-cleavage association of P35 with human caspase-3. Increasing amounts of purified wild-type (wt) P35-$His_6$ (5–50 μg) or $P_1$ (D87A)-mutated P35-$His_6$ (50 μg) were mixed with caspase-3-containing insect cell extracts. P35-$His_6$ and associated proteins subsequently were isolated by metal ($Ni^{2+}$) affinity chromatography and analyzed by SDS–PAGE. Shown are a stained gel (**A**), and immunoblots using antiserum to P35 (**B**) and the p17 (**C**) and p12 (**D**) subunits of caspase-3. Full-length P35 and its N-terminal (∗′) and C-terminal (∗) cleavage products are shown on the top.

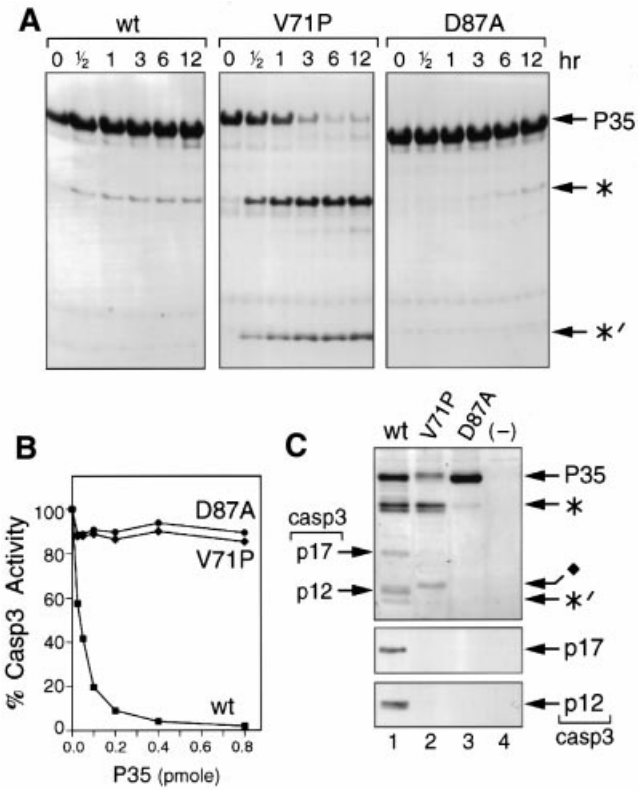


**Fig. 6.** Conversion of P35 from a stoichiometric inhibitor to a non-inhibitory substrate. (**A**) P35 cleavage reactions. Purified wild-type (wt), V71P- or $P_1$ (D87A)-mutated P35-$His_6$ (160 pmol) were mixed with purified caspase-3-$His_6$ (20 pmol). Samples were removed at the indicated times and subjected to SDS–PAGE. A Coomassie-stained gel is shown with P35 and its N-terminal (∗′) and C-terminal (∗) cleavage products indicated on the right. (**B**) P35 inhibition profiles. Increasing amounts of the indicated P35 were mixed with purified caspase-3 (0.2 pmol). After 30 min, residual protease activity was measured by using the tetrapeptide substrate DEVD-AMC in fluorometric assays. Values of a representative experiment are shown as the averages of duplicate determinations expressed as a percentage of total protease activity. (**C**) Association of P35 and caspase-3. After incubation of the indicated P35-$His_6$ (25 μg) with caspase-3-containing insect cell extracts, proteins were isolated by metal ($Ni^{2+}$) affinity chromatography and analyzed as described in the legend to Figure 5. A stained gel (top panel) and immunoblots using antiserum to the p17 and p12 subunits of caspase-3, respectively (bottom panels), are shown. No proteins were detected in the absence of P35-$His_6$ (lane 4).

and p12) associated with wild-type P35-$His_6$ (Figure 5C and D, lanes 1–4), as indicated by their co-purification during metal ($Ni^{2+}$) affinity chromatography. The extent of caspase-3 interaction paralleled the amount of input P35-$His_6$ and the level of P35 cleavage. Moreover, both N- and C-terminal P35 cleavage products co-purified with the complex (Figure 5B), consistent with the hypothesis that their retention contributes to caspase inhibition (Bump *et al.*, 1995). However, no stable association between caspase-3 subunits and D87A-mutated P35-$His_6$ was detected (Figure 5C and D, lane 5). Under these conditions, caspase-3 did not associate with the $Ni^{2+}$ resin in the absence of wild-type P35-$His_6$ (data not shown). Due to the direct correlation between Asp87-dependent cleavage and stable interaction with caspase-3, we concluded that Asp87 is required for complex formation by providing the scissile bond for P35 cleavage or by promoting recognition and initial binding of P35 to the target caspase.

### *Role of the P35 reactive site loop in caspase inhibition*

To investigate these mechanistic possibilities, we determined the effect of distorting the P35 reactive site loop without altering Asp87. Previous mutational studies indicated that two-codon Ala–Ser insertions within the reactive site loop caused P35 loss of function (Bertin *et al.*, 1996). In contrast, charged-to-alanine substitutions of residues comprising the solvent-exposed portion of the reactive site loop (R64, D65, R66, K70, D72, E73, H90, D91, K97, D98 and E99), other than the $P_4$–$P_1$ cleavage residues, had no effect. Thus, the size and orientation of the reactive site loop contribute to caspase inhibition more than surface charge. Since the spatial configuration of the loop is determined in part by the interaction of helix α1 with the β-core (Figure 1), we disrupted α1 by replacing the central residue Val71 with proline, a known helix breaker. This single residue substitution caused P35 loss of function since V71P-mutated P35 failed to prevent baculovirus-induced apoptosis (data not shown). Nonetheless, as demonstrated by *in vitro* protease assays, V71P-mutated P35-$His_6$ is an efficient caspase substrate (Figure 6A). In the presence of purified human caspase-3, an 8-fold molar excess of V71P-mutated P35-$His_6$ was cleaved to

completion. In contrast, wild-type P35-$His_6$ stoichiometrically inhibited caspase-3 as indicated by limited P35 cleavage. Moreover, V71P-mutated P35-$His_6$ failed to inhibit caspase-3 in dose-dependent assays that used the tetrapeptide DEVD-AMC as substrate (Figure 6B). Compared with wild-type P35-$His_6$, V71P-mutated P35-$His_6$ was as ineffective in inhibiting caspase-3 activity as cleavage-deficient D87A-mutated P35-$His_6$. The loss of caspase inhibition correlated with the failure of V71P-mutated P35-$His_6$ to associate stably with caspase-3 (Figure 6C). Wild-type (lane 1), but not V71P-mutated P35-$His_6$ (lane 2), co-purified with p17 and p12 subunits by $Ni^{2+}$ affinity chromatography. Nonetheless, the larger P35 cleavage fragment co-purified with the smaller V71P-containing fragment (◆), which exhibited an altered mobility (lane 2). The association of both cleavage fragments suggested that the overall structure of V71P-mutated P35 was not disrupted even upon caspase cleavage. We concluded that distortion of the reactive site loop converts P35 from a substrate inhibitor to an efficient but non-inhibitory substrate. These data provide the first evidence that P35 residues outside the $P_4$–$P_1$ recognition site participate in caspase inhibition.

## Discussion

The 2.2 Å resolution structure of active P35 prior to caspase cleavage revealed a novel reactive site loop that projects from the main β-sheet core of the protein in an orientation fully accessible to a target caspase (Figure 1). The solvent-exposed configuration of the flexible loop is determined in part by its interactions with the main framework of P35, which includes a CBD of unknown biological function (Figure 2). Our structural and biochemical data indicate a critical role for P35's reactive site loop in a multi-step mechanism for stoichiometric caspase inhibition. Whereas the $P_1$ residue (Asp87) is required for P35 anti-apoptotic activity, cleavage here is not sufficient for stable association with the target caspase or its inhibition. Thus, an additional inhibitory event(s) is required. In light of the limited pre-cleavage contacts modeled between P35 and human caspase-3 (Figure 4), a cleavage-induced conformational change that stabilizes the interaction of P35 with the target caspase probably accounts for the observed high-affinity inhibition. Charged-to-alanine substitutions of residues comprising the solvent-exposed portions of the reactive site loop, including transverse helix α1, had little effect on P35 function (Bertin *et al*., 1996). However, distortion of helix α1 by the substitution V71P eliminated stable association and caspase inhibition without affecting cleavage by the target caspase (Figure 6). These findings suggested that the orientation of the reactive site loop with respect to the main body of P35 is critical for post-cleavage caspase interactions. P35's potency as an inhibitor of all known caspase groups suggests that a structural or mechanistic feature shared among the diverse caspases contributes to such interactions. Further studies are required to define the molecular contacts between P35 and protease in the complex.

Despite the lack of sequence similarity between P35 and the serpins (serine protease inhibitors), the P35 reactive site loop may be functionally analogous to the reactive center of the serpins. Protease inhibition by the serpins involves cleavage-induced conformational changes (Carrell *et al*., 1994; Schreuder *et al*., 1994) that promote formation of a detergent-stable complex (reviewed in Whisstock *et al*., 1998). To date, the molecular interactions between serpin and target protease in the inhibited complex remain unresolved. Although it is not yet known whether pre-cleaved P35 inhibits caspase activity, the functional analogy between serpin and P35 reactive sites suggests that a vulnerable loop may be a common mechanistic feature of cleavage-dependent protease inhibitors, irrespective of protease class or specificity. Nonetheless, it is noteworthy that the mechanism of P35-mediated suicide inhibition is distinct from that of the serpins. Although quite stable, the inhibited P35–caspase complex is detergent labile. Moreover, P35 exhibits a universal specificity for caspases, but excludes non-caspase proteases (Bump *et al*., 1995; Xue and Horvitz, 1995; Bertin *et al*., 1996; Ahmad *et al*., 1997; Zhou *et al*., 1998). Thus, P35 is distinguished from the cowpox virus serpin CrmA, which is a highly selective caspase inhibitor (Pickup *et al*., 1986; Zhou *et al*., 1998).

The three-dimensional structure of P35 offers new insights into mechanisms of protease inhibition, specifically that of the caspases. The rational design of new P35-based inhibitors with the potential for increased selectivity among classes of caspases is now possible. Such discrimination between death proteases would be a requirement for strategies of *in vivo* caspase inactivation when used in therapeutic approaches (Jacobson, 1998) for treatment of inflammatory and apoptosis-associated diseases.

## Materials and methods

### *Protein expression and crystallization*

P35 from the baculovirus *Autographa californica* nucleopolyhedrovirus (AcMNPV) strain L1 was cloned into an *Escherichia coli* pET vector expression system (Novagen, Madison, WI) resulting in expression of protein with a C-terminal His-Tag extension (P35-$His_6$). Cloning, expression and protein purification details are described elsewhere (Bertin *et al*., 1996). Recombinant His-tagged P35 protein inhibited apoptosis in a similar fashion to wild-type (Bertin *et al*., 1996). P35-$His_6$ protein was crystallized by hanging-drop vapor diffusion and by microbatch at 4°C in 1.5–2.0 M $Na^+/K^+$ $PO_4$, 100 mM NaCl, 1% ethylene glycol, pH 7.0. The final protein concentration was 5–10 mg/ml. The crystals grew to the size of 0.7×0.2×0.2 mm in 4 weeks and belong to the orthorhombic space group $C222_1$ with unit cell parameters of $a$ = 114.6 Å, $b$ = 130.1 Å, $c$ = 181.1 Å. A $V_M$ coefficient was calculated to be 2.41 $Å^3$/Da (49% solvent) assuming two P35 homodimers per asymmetric unit (ASU) (Matthews, 1968). Dynamic light scattering data suggest that P35 forms homodimers in solution (data not shown). However, initial low-resolution electron density maps phased by multiple isomorphous derivatives produced three regions of protein density. Three P35 monomers/ASU results in a $V_M$ of 3.21 $Å^3$/Da and a solvent content of 62% by volume.

Crystals were transferred to 1.8 M $Na^+/K^+$ $PO_4$, 200 mM NaCl, 30% ethylene glycol and frozen to –170°C for data collection. Native and derivative data were collected on a Siemens Hi-Star and MSC Raxis-IV mounted on Rigaku rotating anode generators. Hi-Star data were processed with XDS (Kabsch, 1988) and scaled with ROTAVATA/AGROVATA (CCP4, 1994). Raxis-IV data were processed with DENZO and scaled with SCALEPACK (Otwinowski and Minor, 1997). A 2.2 Å resolution native data set was collected on Beamline 7-1 at SSRL and processed with DENZO and SCALEPACK.

### *Phase determination*

All heavy atoms soaks were conducted at 4°C in 1.8 M $Na^+/K^+$ $PO_4$, 100 mM NaCl, 1% ethylene glycol, pH 7.0. Heavy atom positions were determined by inspection of difference Patterson maps and difference

**Table I.** Data collection, phasing and refinement statistics

| | Data set | | | |
|---|---|---|---|---|
| | Native 1 | Native 2 | $KAu(CN)_2$ | $LuCl_3$ |
| X-ray source | SSRL | Cu-Kα | Cu-Kα | Cu-Kα |
| Wavelength (Å) | 1.08 | 1.54 | 1.54 | 1.54 |
| Resolution (Å) | 2.2 | 2.5 | 2.9 | 3.0 |
| No. of observations | 324 073 | 182 892 | 189 129 | 151 939 |
| No. of unique reflections | 66 997 | 46 005 | 27 507 | 25 920 |
| Completeness (%) | 97.8 | 97.5 | 91.8 | 95.2 |
| $R_{merge}$[1] (%) | 6.4 | 6.6 | 6.3 | 7.3 |
| Heavy atom concentration (mM) | | | 0.1 | 10.0 |
| Soaking time (days) | | | 2 | 8 |
| No. of sites (ASU) | | | 4 | 2 |
| $R_{iso}$[b] (%) | | | 11.7 | 7.5 |
| Phasing power[c] | | | 2.03 | 1.20 |
| Figure of merit | | | 0.521 | |
| *Refinement statistics* | | | | |
| Resolution | 30.0–2.2 Å | | | |
| No. of reflections ($\|F\| \geqslant 0$) | 66 997 | | | |
| *R*-factor[d] | 19.6 | | | |
| $R_{free}$[d] (5% data) | 26.0 | | | |
| R.m.s. bond distances | 0.018Å | | | |
| R.m.s. bond angles | 2.04° | | | |
| Non-hydrogen atoms | 7538 | | | |

[a]$R_{merge} = [\Sigma_h\Sigma_i|I_h - I_{hi}|/\Sigma_h\Sigma_i I_{hi}]\times100$ where $I_h$ is the mean of the $I_{hi}$ observations of reflection *h*.
[b]$R_{iso} = \Sigma||F_{PH}| - |F_P||/\Sigma|F_{PH}|\times100$.
[c]Phasing power $= [\Sigma_h|F_{H(calc)}|^2/\Sigma_h(|F_{PH(obs)}| - |F_{PH(calc)}|)^2]^{1/2}$.
[d]*R*-factor and $R_{free} = \Sigma||F_{obs}| - |F_{calc}||/\Sigma|F_{obs}|\times100$ for 95% of recorded data (*R*-factor) or 5% of data ($R_{free}$).

Fourier maps. The heavy atom positions were refined and MIR phases calculated using the program PHASES (Furey and Swaminathan, 1997). Phasing statistics are listed in Table I. The MIR pases were refined by 3-fold molecular averaging and solvent flattening using the RAVE software package (Kleywegt and Jones, 1994). The preliminary NCS rotation matrices were determined by rotation of the initial skeletonized solvent-flattened MIR electron density map. After 15 rounds of molecular averaging and solvent flattening at 2.9 Å resolution, the averaging *R*-factor dropped to 21.5% with a correlation coefficient of 0.907.

### *Model building and refinement*

The 3-fold averaged electron density map was readily interpretable and a single monomer was built into the density with aid of the molecular graphics program O (Jones *et al*., 1991). Residues corresponding to the solvent-exposed portion of the reactive site loop (84–95) were disordered in the original averaged map. After initial model building, the complete asymmetric unit was generated by rotating and translating the monomer built in the averaged map. The structure was refined with non-crystallographic constraints using TNT (Tronrud *et al*., 1987). After the first round of refinement, the conventional *R*-factor dropped to 31.5% for 95% of the recorded data between 30 and 2.9 Å resolution (working data set). The new electron density map allowed the tracing of additional residues in the reactive site loop. At this stage, the model was refined against synchrotron data, slowly extending the resolution with each round to a final resolution of 2.2 Å. The working and test data sets maintained the same lower resolution reflections upon extension. After several iterative rounds of refinement followed by manual re-building, the non-crystallographic refinement constraints were relaxed, which resulted in a drop of 1.1% in the $R_{free}$ value for 5% of all recorded data. The model was then subjected to subsequent rounds of simulated annealing with the program CNS (Brunger *et al*., 1998), applying the maximum likelihood as a refinement target. The working and test data sets were identical to TNT refinement. The final conventional *R*-factor is 19.6% and the $R_{free}$ value is 26.0% for 95 and 5% of all recorded data, respectively (Brunger, 1992). None of the 892 residues in the asymmetric unit plot in the disallowed region of the Ramachandran plot, and 98.7% of the residues lie in the most favored or additionally allowed regions as defined by the program PROCHECK (Laskowski *et al*., 1993).

### *P35–caspase assays*

For caspase association assays, purified wild-type or mutated P35-$His_6$ was mixed with clarified, freeze–thaw extracts of ~$3\times10^6$ *Spodoptera frugiperda* (Sf21) cells inoculated 48 h previously with a baculovirus vector expressing the human caspase-3 gene (Fernandes-Alnemri *et al*., 1994). After 30 min, the reactions were diluted with binding buffer (20 mM Tris pH 7.9, 0.5 M NaCl, 5 mM imidazole) and subjected to metal affinity chromatography by using $Ni^{2+}$-conjugated agarose beads. Bound proteins were eluted with binding buffer containing 1 M imidazole and analyzed by SDS–PAGE and staining with colloidal Coomassie G250 or immunoblotting with polyclonal rabbit antisera to P35, or p17 and p12 subunits of caspase-3. Immunoblots were developed by using goat anti-rabbit immunoglobulin G (Pierce) conjugated to alkaline phosphatase. D87A-mutated P35 was described previously (Bertin *et al*., 1996). Overlap extension PCR using complementary primers 5′-AGAATAAAATCAAAACCGGATGAACAATTTGAT-3′ and 5′-ATCAAATTGTTCATCCGGTTTTGATTTTATTCT-3′ were used to generate pET-22B containing *p35* for production of V71P-mutated P35-$His_6$. The codon substitution was verified by nucleotide sequencing. For cleavage assays, wild-type or mutated P35-$His_6$ was mixed with purified human caspase-3 in 100 mM HEPES (pH 7.5), 0.1% CHAPS and 10% sucrose. C-terminal $His_6$-tagged caspase-3 was purified by overexpression in *E.coli* and metal affinity chromatography. Reaction products were analyzed by electrophoresis on 10–20% polyacrylamide gradient gels followed by staining. For protease inhibition assays, P35-$His_6$ was mixed with purified caspase-3 (200 fmol) using reaction conditions described elsewhere (Bertin *et al*., 1996). After 30 min, the tetrapeptide substrate Ac-DEVD-AMC (Peptides International) was added to 10 μM and the accumulation of fluorescent product (excitation, 360 nm; emission, 465 nm) was monitored by using a Biolumin 960 microplate reader (Molecular Dynamics). Rates of product formation were obtained over the first 10% of substrate depletion, and percentage protease activity is reported as the ratio of the calculated rates in the presence and absence of P35-$His_6$.

## Acknowledgements

We are grateful to I.Rayment for providing facilities and resources during the preliminary stages of this work. E.Baker and C.Smith are

acknowledged for sharing synchrotron time. We thank the staff at SSRL. J.Beynon and M.Eddins are recognized for assistance in protein acquisition. We also thank J.Bertin for initial characterization of P35-$His_6$. This work is funded by NIH grants GM56774 to A.J.F., AI40482 to P.D.F., and the W.M.Keck Foundation Center for Structural Biology at UC-Davis. Coordinates have been deposited in the Brookhaven Protein Databank, access code: 1P35.

## References

Ahmad,M., Srinivasula,S.M., Wang,L., Litwack,G., Fernandes-Alnemri,T. and Alnemri,E.S. (1997) *Spodoptera frugiperda* caspase-1, a novel insect death protease that cleaves the nuclear immunophilin FKBP46, is the target of the baculovirus anitiapoptotic protein P35. *J. Biol. Chem.*, **272**, 1421–1424.

Beidler,D.R., Tewari,M., Friesen,P.D., Poirier,G. and Dixit,V.M. (1995) The baculovirus P35 protein inhibits Fas- and tumor necrosis factor-induced apoptosis. *J. Biol. Chem.*, **270**, 16526–16528.

Bertin,J., Mendrysa,S.M., LaCount,D.J., Gaur,S., Krebs,J.F., Armstrong,R.C., Tomaselli,K.J. and Friesen,P.D. (1996) Apoptotic suppression by baculovirus P35 involves cleavage by and inhibition of a virus-induced CED-3/ICE-like protease. *J. Virol.*, **70**, 6251–6259.

Brunger,A.T. (1992) The free *R* value: a novel statistical quantity for assessing the accuracy of crystal structures. *Nature*, **355**, 472–474.

Brunger,A.T. *et al*. (1998) Crystallography and NMR system: a new software suite for macromolecular structure determination. *Acta Crystallogr.*, **D54**, 905–921.

Bump,N.J. *et al*. (1995) Inhibition of ICE protease by baculovirus antiapoptotic protein P35. *Science*, **269**, 1885–1888.

Carrell,R.W., Stein,P.E., Fermi,G. and Wardell,M.R. (1994) Biological implications of a 3 Å structure of dimeric antithrombin. *Structure*, **2**, 257–270.

Cartier,J.L., Hershberger,P.A. and Friesen,P.D. (1994) Suppression of apoptosis in insect cells stably transfected with baculovirus P35: dominant interference by N-terminal sequences P351–76. *J. Virol.*, **68**, 7728–7737.

CCP4 (1994) The CCP4 suite: programs for protein crystallography. *Acta Crystallogr.*, **D50**, 760–763.

Clem,R.J., Fechheimer,M. and Miller,L.K. (1991) Prevention of apoptosis by a baculovirus gene during infection of insect cells. *Science*, **254**, 1388–1390.

Cryns,V. and Yuan,J. (1998) Proteases to die for. *Genes Dev.*, **12**, 1551–1570.

Davidson,F. and Steller,H. (1998) Blocking apoptosis prevents blindness in *Drosophila* retinal degeneration mutants. *Nature*, **391**, 587–591.

Fernandes-Alnemri,T., Litwack,G. and Alnemri,E.S. (1994) CPP32, a novel human apoptotic protein with homology to *Caenorhabditis elegans* cell death protein Ced-3 and mammalian interleukin-1 beta-converting enzyme. *J. Biol. Chem.*, **269**, 30761–30764.

Fraser,A. and Evan,G. (1996) A license to kill. *Cell*, **85**, 781–784.

Furey,W. and Swaminathan,S. (1997) PHASES-95: a program package for the processing and analysis of diffraction data from macromolecules. *Methods Enzymol.*, **277**, 590–620.

Hardwick,J.M. (1997) Virus-induced apoptosis. *Adv. Pharmacol*., **41**, 295–336.

Hay,B.A., Wolff,T. and Rubin,G.M. (1994) Expression of baculovirus P35 prevents cell death in *Drosophila*. *Development*, **120**, 2121–2129.

Hengartner,M.O. and Horvitz,H.R. (1994) Programmed cell death in *Caenorhabditis elegans*. *Curr. Opin. Genet. Dev.*, **4**, 581–586.

Holm,L. and Sander,C. (1993) Protein structure comparison by alignment of distance matrices. *J. Mol. Biol.*, **233**, 123–138.

Jacobson,M.D. (1998) Anti-apoptosis therapy: a way of treating neural degeneration? *Curr. Biol.*, **8**, 418–421.

Jacobson,M.D., Weil,M. and Raff,M.C. (1997) Programmed cell death in animal development. *Cell*, **88**, 347–354.

Jones,T.A., Zou,J.Y., Cowan,S.W. and Kjeldgaard,M. (1991) Improved methods for the building of protein models in electron density maps and the location of errors in these models. *Acta Crystallogr.*, **A47**, 110–119.

Kabsch,W. (1976) A solution for the best rotation to relate two sets of vectors. *Acta Crystallogr.*, **A32**, 922–923.

Kabsch,W. (1988) Evaluation of single-crystal X-ray diffraction data from a position sensitive detector. *J. Appl. Crystallogr.*, **21**, 916–924.

Kleywegt,G.J. and Jones,T.A. (1994) Halloween... masks and bones. From first map to final model. *CCP4*. Daresbury, UK, pp. 59–66.

Kraulis,P.J. (1991) MOLSCRIPT: a program to produce both detailed and schematic plots of protein structures. J. *Appl. Crystallogr.*, **24**, 946–950.

Laskowski,R.A., MacArthur,M.W., Moss,D.S. and Thornton,J.M. (1993) PROCHECK: a program to check the stereochemical quality of protein structures. *J. Appl. Crystallogr.*, **26**, 283–291.

Martin,S.J. and Green,D.R. (1995) Protease activation during apoptosis: death by a thousand cuts? *Cell*, **82**, 349–352.

Martinou,I., Fernandez,P.A., Missotten,M., White,E., Allet,B., Sadoul,R. and Martinou,J.C. (1995) Viral proteins E1B19K and P35 protect sympathetic neurons from cell death induced by NGF deprivation. *J. Cell Biol.*, **128**, 201–208.

Matthews,B.W. (1968) Solvent content of protein crystals. *J. Mol. Biol.*, **33**, 491.

Mittl,P., Di Marco,S.,.. Krebs,J., Bai,X., Karanewsky,D., Priestle,J., Tomaselli,K. and Grutter,M. (1997) Structure of recombinant human CPP32 in complex with the tetrapeptide acetyl-Asp-Val-Ala-Asp fluoromethyl ketone. *J. Biol. Chem.*, **272**, 6539–6547.

Nicholls,A., Sharp,K.A. and Honig,B. (1991) Protein folding and association: insights from the interfacial and thermodynamic properties of hydrocarbons. *Proteins: Struct., Funct. Genet*., **11**, 281–296.

Nicholson,D.W. and Thornberry,N.A. (1997) Caspases: killer proteases. *Trends Biochem. Sci.*, **22**, 299–306.

O'Brien,V. (1998) Viruses and apoptosis. *J. Gen. Virol.*, **79**, 1833–1845.

Otwinowski,Z. and Minor,W. (1997) Processing of X-ray diffraction data collected in oscillation mode. *Methods Enzymol.*, **276**, 307–326.

Pickup,D.J., Ink,B.S., Hu,W., Ray,C.A. and Joklik,W.K. (1986) Hemorrhage in lesions caused by cowpox virus is induced by a viral protein that is related to plasma protein inhibitors of serine proteases. *Proc. Natl Acad. Sci. USA*, **83**, 7698–7702.

Rabizadeh,S., LaCount,D.J., Friesen,P.D. and Bredesen,D.E. (1993) Expression of the baculovirus P35 gene inhibits mammalian neural cell death. *J. Neurochem*., **61**, 2318–2321.

Robertson,N.M., Zangrilli,J., Fernandes-Alnemri,T., Friesen,P.D., Litwack,G. and Alnemri,E.S. (1997) Baculovirus P35 inhibits the glucocorticoid-mediated pathway of cell death. *Cancer Res.*, **57**, 43–47.

Rotonda,J. *et al*. (1996) The three-dimensional structure of apopain/CPP32, a key mediator of apoptosis. *Nature Struct. Biol.*, **3**, 619–625.

Schreuder,H., de Boer,B., Dijkema,R., Mulders,J., Theunissen,H., Grootenhuis,P. and Hol,W. (1994) The intact and cleaved human antithrombin III complex as a model for serpin–proteinase interactions. *Nature Struct. Biol*., **1**, 48–54.

Shen,Y. and Shenk,T.E. (1995) Viruses and apoptosis. *Curr. Opin. Genet. Dev.*, **5**, 105–111.

Smith,T.J. (1995) MolView: a program for analyzing and displaying atomic structures on the Macintosh personal computer. *J. Mol. Graphics*, **13**, 122–125.

Steller,H. (1995) Mechanisms and genes of cellular suicide. *Science*, **267**, 1445–1449.

Sugimoto,A., Friesen,P.D. and Rothman,J.H. (1994) Baculovirus P35 prevents developmentally programmed cell death and rescues a *ced-9* mutant in the nematode *Caenorhabditis elegans*. *EMBO J.*, **13**, 2023–2028.

Thompson,C.B. (1995) Apoptosis in the pathogenesis and treatment of disease. *Science*, **267**, 1456–1462.

Tronrud,D.E., Ten-Eyck,L.F. and Matthews,B.W. (1987) An efficient general-purpose least-squares refinement program for macromolecular structures. *Acta Crystallogr.*, **A43**, 489–501.

Villa,P., Kaufmann,S.H. and Earnshaw,W.C. (1997) Caspases and caspase inhibitors. *Trends Biochem. Sci.*, **22**, 388–393.

Whisstock,J., Skinner,R. and Lesk,A. (1998) An atlas of serpin conformations. *Trends Biochem. Sci.*, **23**, 63–67.

White,E. (1996) Life, death and the pursuit of apoptosis. *Genes Dev.*, **10**, 1–15.

Xu,G.-Y., Ong,E., Gilkes,N.R., Kilburn,D.G., Muhandiram,D.R., Harris-Brandts,M., Carver,J.P., Kay,L.E. and Harvey,T.S. (1995) Solution structure of a cellulose-binding domain from *Cellulomonas fimi* by nuclear magnetic resonance spectroscopy. *Biochemistry*, **34**, 6993–7009.

Xue,D. and Horvitz,R. (1995) Inhibition of the *Caenorhabditis elegans* cell-death protease CED-3 by a CED-3 cleavage site in baculovirus P35 protein. *Nature*, **377**, 248–251.

Zhou,Q., Krebs,J.F., Snipas,S.J., Price,A., Alnemri,E.S., Tomaselli,K.J. and Salvesen,G.S. (1998) Interaction of the baculovirus anti-apoptotic protein P35 with caspases. Specificity, kinetics and characterization of the caspase/P35 complex. *Biochemistry*, **37**, 10757–10765.

*Received December 22, 1998; revised and accepted February 19, 1999*